Quantitative and Statistical Study of the Dynamics of Clathrin-Dependent and -Independent Endocytosis Reveal a Differential Role of EndophilinA2

Laetitia Bertot, Alexandre Grassart, Thibault Lagache, Giacomo Nardi, Cyril Basquin, Jean-Christophe Olivo-Marin, Nathalie Sauvonnet

Article

Cell Reports

Quantitative and Statistical Study of the Dynamics of Clathrin-Dependent and -Independent Endocytosis Reveal a Differential Role of EndophilinA2

Graphical Abstract

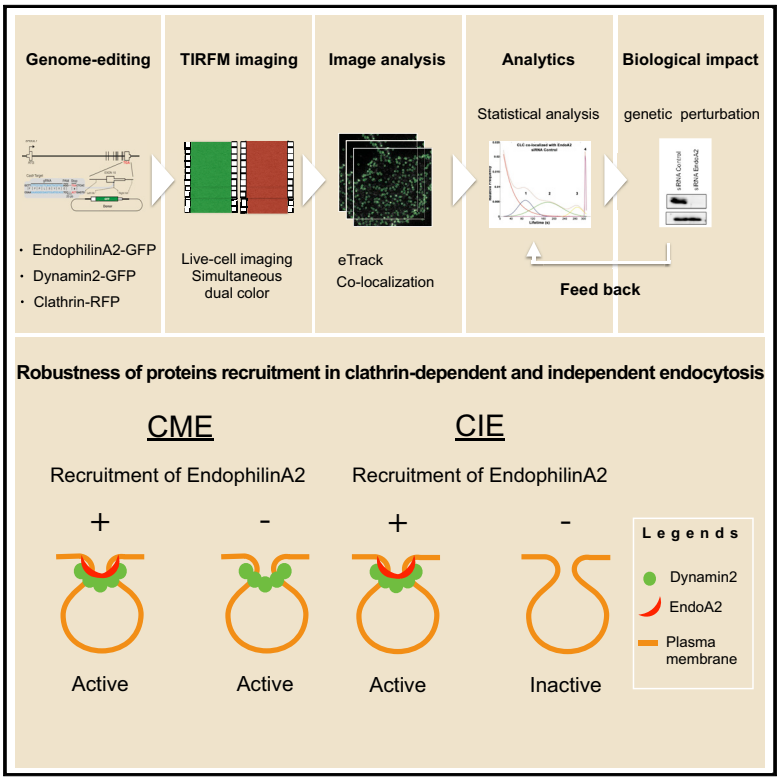

Highlights

- Native dynamics of endophilinA2 and dynamin2 followed in CME and CIE
- Analytics of subpopulation dynamics reveal similarities between CME and CIE
- Dynamin2:endophilinA2 stoichiometry is conserved between CME and CIE
- EndophilinA2 is essential for dynamin2 recruitment only in CIE

Authors

Laetitia Bertot, Alexandre Grassart, Thibault Lagache, Giacomo Nardi, Cyril Basquin, Jean-Christophe Olivo-Marin, Nathalie Sauvonnet

Correspondence

nathalie.sauvonnet@pasteur.fr

In Brief

Bertot et al. interrogate endophilinA2 dynamics and interplay with dynamin2 in clathrin-mediated (CME) and -independent (CIE) endocytosis. The work shows that endophilinA2 is a conserved endocytic factor in both pathways, acting with dynamin in a similar stoichiometry, but its presence is required only in CIE for dynamin2 recruitment.

Bertot et al., 2018, Cell Reports 22, 1574–1588
February 6, 2018
https://doi.org/10.1016/j.celrep.2018.01.039

CellPress

OPEN ACCESS
CellPress

Cell Reports
Article

Quantitative and Statistical Study of the Dynamics of Clathrin-Dependent and -Independent Endocytosis Reveal a Differential Role of EndophilinA2

Laetitia Bertot,[1,5] Alexandre Grassart,[1,5] Thibault Lagache,[2,4,5] Giacomo Nardi,[2,5] Cyril Basquin,[3] Jean-Christophe Olivo-Marin,[2] and Nathalie Sauvonnet[1,6,*]

[1]Unité de Pathogénie Microbienne Moléculaire, Institut Pasteur, INSERM U1202. 28, rue du Docteur Roux, 75015 Paris, France
[2]Unité d'Analyse d'Images Biologiques, Institut Pasteur, CNRS UMR3691. 25, rue du Docteur Roux, 75015 Paris, France
[3]Institut Jacques Monod, Equipe de Polarité Cellulaire dans le Développement et l'évolution, CNRS UMR 7592. 15, rue Hélène Brion, 75205 Paris Cedex 13, France
[4]Present address: Department of Biological Sciences, Columbia University, New York, NY 10027, USA
[5]These authors contributed equally
[6]Lead Contact
*Correspondence: nathalie.sauvonnet@pasteur.fr
https://doi.org/10.1016/j.celrep.2018.01.039

SUMMARY

Eukaryotic cells internalize cargos specifically through clathrin-mediated endocytosis (CME) or clathrin-independent endocytosis (CIE). EndophilinA2 was shown as preferentially implicated in CIE, although initially involved in CME. Here, we investigated the native interplay of endophilinA2 and dynamin2 during CME as compared to CIE. We developed an unbiased integrative approach based on genome engineering, robust tracking methodology, and advanced analytics. We statistically identified CME and CIE subpopulations corresponding to abortive, active, and static endocytic events. Depletion of dynamin2 strongly affected active CME and CIE events, whereas the absence of endophilinA2 impacted only CIE. Accordingly, we demonstrated that endophilinA2 is needed for dynamin2 recruitment during CIE, but not in CME. Despite these differences, endophilinA2 and dynamin2 acted at the latest stage of endocytosis within a similar stoichiometry in both mechanisms. Thus, we propose a conserved function of dynamin2 and endophilinA2 in vesicle scission, but a differential regulation of their recruitment during CME and CIE.

INTRODUCTION

Different endocytosis pathways have been identified in eukaryotic cells among which clathrin-mediated endocytosis (CME) remains the most extensively studied. Several clathrin-independent endocytosis (CIE) processes have been also uncovered and further classified upon their dependency to the GTPase dynamin. The interleukin-2 (IL-2) receptors (IL-2Rs) (both β and γ chains) were among the first physiological examples of cargos taken up by CIE and requiring dynamin (Lamaze et al., 2001; Sauvonnet et al., 2005; Subtil et al., 1994). Interestingly, these receptors can be internalized constitutively (without the ligand) or in the presence of IL-2 (Hémar et al., 1995; Subtil et al., 1997). Thus, studying the constitutive internalization of IL-2R represents an effective strategy for understanding CIE endocytic mechanism disengaged from receptor signaling.

So far, about 15 factors have been implicated in the uptake of IL-2R (Basquin et al., 2015; Grassart et al., 2008; 2010). Among them, dynamin2 (Dnm2) and endophilinA2 (EndoA2) have been implicated in other endocytic pathways (Basquin et al., 2015; Sauvonnet et al., 2005). Recently, the role of the BAR domain protein endophilin has been the subject of many investigations and debates (Ferguson et al., 2009; Frost et al., 2009; Meinecke et al., 2013; Suetsugu, 2016). Indeed, based on *in vitro* studies, at least three different functions have been proposed: (1) recruitment of cargo or endocytic protein-like dynamin via its SH3 domain (Boucrot et al., 2015; Milosevic et al., 2011; Tang et al., 1999), (2) membrane curvature via its BAR domain, and (3) membrane binding and vesicle fission via its amphipathic helices (Renard et al., 2015). *In vivo*, endophilins have been initially involved in CME (Antonny, 2006; Antonny et al., 2016; Farsad et al., 2001; Perera et al., 2006). More recently, it has been also proposed that EndoA2 might actually work preferentially in CIE pathways (Boucrot et al., 2015; Renard et al., 2015). In both pathways, how endophilin is recruited and functions *in vivo* remain poorly understood.

Interestingly, a recent *in vitro* study indicates that an excessive endophilin concentration inhibits dynamin-mediated fission of reconstituted lipid nanotube (Hohendahl et al., 2017). Thus, studying EndoA2 dynamics in cells through classical gene overexpression might disrupt its native localization but also impact its function. It is in this context that we decided to interrogate EndoA2 dynamics, function, and interplay with Dnm2 in CME and CIE within a preserved physiological environment. To do so, we engineeried genome-edited cells to produce native GFP/RFP fusion protein of EndoA2, Dnm2, and clathrin light chain A (CLC). We associated this approach with an advanced imaging and analysis pipeline and the measurement of protein stoichiometry in living cell during CME and CIE.

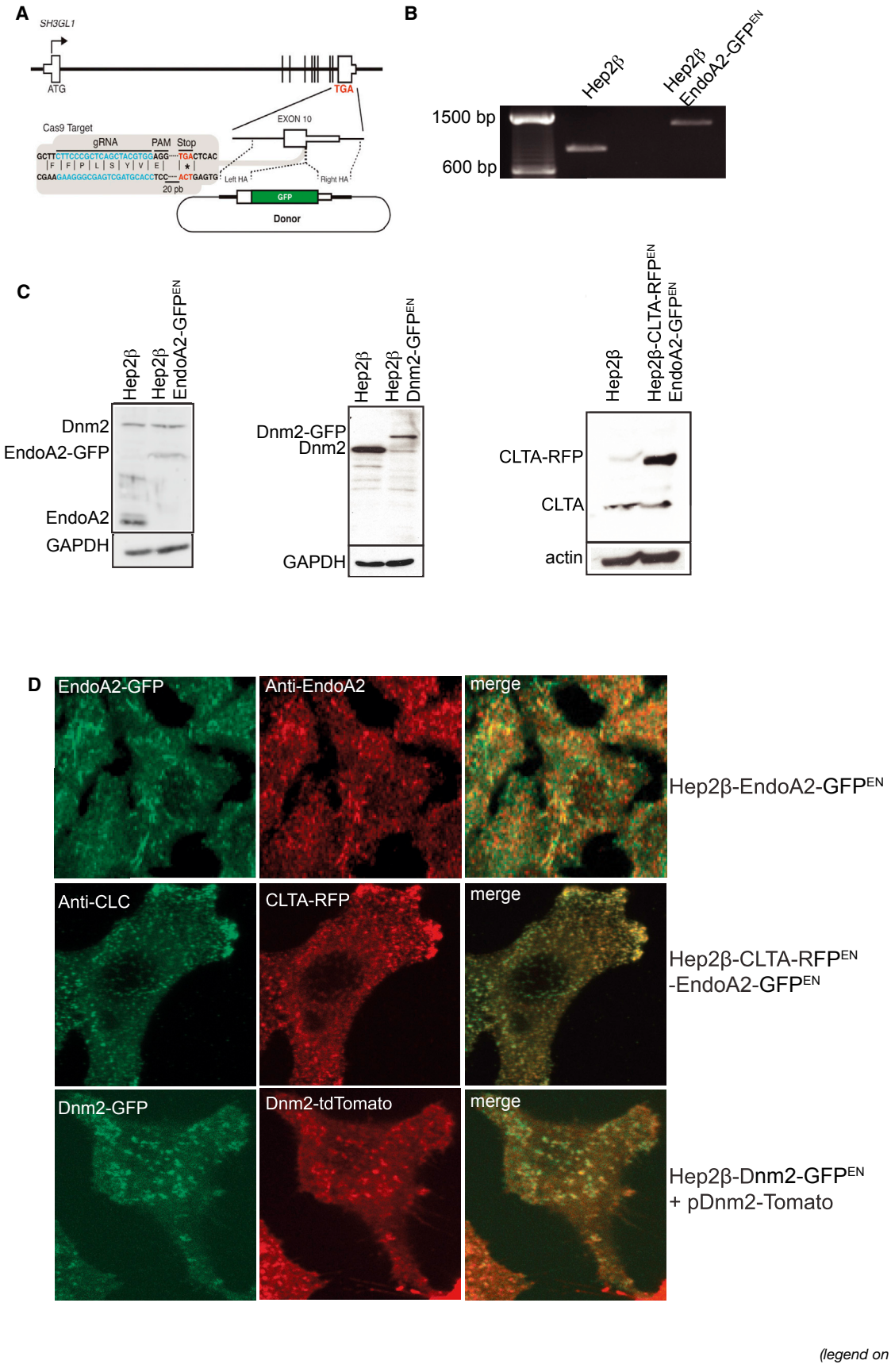

(legend on next page)

RESULTS

Generation of Genome-Edited Cells for EndoA2-GFP, Dnm2-GFP, and CLC-RFP

To verify the implication of endophilin in the constitutive uptake of IL-2R, we knocked down endophilinA1 (EndoA1) and/or EndoA2 by small interfering RNAs (siRNA) in Hep2β cells, an established epithelial cell line stably expressing only the β chain of IL-2R (IL-2Rβ). We observed that the depletion of EndoA1 and/or A2 clearly inhibited IL-2Rβ entry up to 50%, as quantified by Icy software (Basquin et al., 2015; de Chaumont et al., 2012), without affecting the internalization of transferrin (Tf, a bona fide CME marker) (Figures S1A–S1C). The inhibition of IL-2R was equivalent in either single- or double-knockdown cells for EndoA1 and EndoA2, hence indicating that endophilins do not have a compensatory effect. These results show the involvement of endophilins in constitutive endocytosis of IL-2R, and they confirm its preferential implication in CIE rather than CME.

To get deeper insight into the role of endophilins during CME and CIE, we produced EndoA2-GFP genome-edited cells, and we tracked fluorescent spots with total internal reflection fluorescence (TIRF) microscopy. As dynamin is a well-known interacting factor of endophilin, we also analyzed the interplay between these two factors and genome-edited cells for the Dnm2 gene. The advantage of genome editing is to avoid complications due to overexpression, since it preserves the native expression, stoichiometry, and localization of the protein. In contrast, EndoA2 overexpression induces massive tubulation, protein mislocalization, and defective vesicle scission, and it might unbalance protein recruitment to endocytosis sites (Figures S1D and S1E) (Hohendahl et al., 2017).

We used Cas9/CRISPR technology to edit the genome of Hep2β cells and express EndoA2 (SH3GL1) fused to an EGFP. Briefly, EGFP was inserted at the 3′ end of SH3GL1 gene to obtain a C-terminal protein fusion to EGFP, EndoA2-GFP (Figure 1A). Edited single-cell-derived clones were obtained by cell sorting and subsequently analyzed by PCR, western blots, and finally sequenced. We selected a clone bearing all alleles edited (Hep2β-EndoA2-GFP^{EN}), confirmed at both genomic (Figure 1B) and protein (Figure 1C) levels. Furthermore, we confirmed by immunofluorescence a normal distribution of EndoA2-GFP that was co-labeled with an anti-EndoA2 antibody (Pearson coefficient > 0.6; Figure 1D). This co-labeling was good, but not perfect, due to some unspecific component of the antibody when used for immunocytochemistry. Then, we similarly engineered the clathrin light chain A gene (CLTA) to be expressed in Hep2β-EndoA2-GFP^{EN} cells using zinc finger nucleases (ZFNs) (Figures 1C and 1D). Thus, the derived clone expressed both endogenously CLC-RFP and EndoA2-GFP. Finally, we also engineered the Dnm2 gene in Hep2β cells using ZFNs to express a Dnm2-GFP fusion protein (Figures 1C and 1D). Altogether, these gene-edited cell lines allowed us to analyze the native dynamics of EndoA2 and its functional interplay with Dnm2 during CIE and CME processes.

Automated Detection of CIE and CME Sites in Live-Cell TIRF Imaging

To analyze the orchestration of Dnm2 and EndoA2 during CME and CIE, we observed the dynamics of clathrin (CLC) and IL-2Rβ at the plasma membrane of gene-edited cells with time-lapse, TIRF microscopy. As compared to overexpressed conditions, fluorescent spots in genome-edited cells (native conditions) are dimmer, leading to many missed or false spot detections. As a result, standard tracking algorithms usually shorten endocytic tracks (Aguet et al., 2013). We took advantage of the high confinement of fluorescent spots over time to determine the positions of putative endocytic sites very precisely and reconstruct endocytic tracks robustly (Supplemental Experimental Procedures; Figure S2; Movies S1, S2, S3, S4, S5, S6, and S7). We implemented this tracking method (plugin eTrack) in the open-source image analysis software Icy (http://icy.bioimageanalysis.org/) (de Chaumont et al., 2012). We compared eTrack to a state-of-the-art tracking algorithm (enhanced Multiple Hypothesis Tracking [eMHT] method; Chenouard et al., 2014), and we observed that the shortest tracks (<40 s) were diminished by 30% with eTrack (42% of the tracks) compared to eMHT (54.8% of tracks) for clathrin-coated structures and was similar (61%) for IL-2R. We also observed that the number of tracks with a large total displacement (>0.5 μm), which shall correspond to tracks with false step-by-step associations leading to artifactual spot motion, was drastically diminished with eTrack (3.0% for clathrin and 3.5% for IL-2R) compared to eMHT (9.8% for clathrin and 7.8% for IL-2R). We thus conclude that tracks obtained with eTrack are more confined and longer than tracks obtained with other tracking methods, which better corresponds to the confined and long-lasting endocytic process.

Finally, the association of eTrack with object-based co-localization analysis (Lagache et al., 2015) allowed the robust identification of a bank of CLC and IL-2R tracks co-localized or not with either Dnm2 or EndoA2.

Different Recruitment of Dnm2 and EndoA2 in CME Compared to CIE

To better understand the role and the interplay of Dnm2 and EndoA2 during CME and CIE, we analyzed their recruitment in each endocytosis pathway; representative examples are shown in kymographs presented in Figure S3A. We quantified

Figure 1. Generation of Gene Editing of *SH3GL1* Using CRISPR/Cas9 in Hep2β Cells

(A) Schematic representation of the strategy for integration of GFP at the *SH3GL1* locus (EndoA2).

(B) Out-out PCR showing targeted integration of GFP. Control, parental cell line (Hep2β); EndoA2-GFP^{EN}, tagged genome-edited Hep2β cell line.

(C) Western blots analysis of Hep2β (control) and Hep2β EndoA2-GFP^{EN}, Hep2β-Dnm2-GFP^{EN}, and Hep2β-CLC-RFP^{EN}/EndoA2-GFP^{EN} cell lysates immunoblotted with anti-EndoA2, anti-Dnm2, anti-CLTA, and anti-GAPDH.

(D) Immunofluorescence of Hep2β EndoA2-GFP^{EN}, Hep2β-CLC-RFP^{EN}/EndoA2-GFP^{EN}, and Hep2β-Dnm2-GFP^{EN} transfected transiently with pDnm2-tdTomato. Cells were fixed and immunolabeled either using rabbit anti-EndoA2 and secondary anti-rabbit coupled to Alexa 561 (red) or with anti-CLC (con1) and secondary anti mouse-Alexa 488 (green). EndoA2-GFP^{EN}, Dnm2-GFP^{EN} (green), CLC-RFP^{EN}, Dnm2-Tomato (red), and merged pictures are shown.

the co-localization rate between either CLC or IL-2R with Dnm2 or EndoA2 in the respective presence or not of the two latter proteins (i.e., in cells depleted or not for Dnm2 or EndoA2). For CLC tracks, we observed around 80% of co-localization with Dnm2 (Figure S3B). This high rate of Dnm2 recruitment agrees with past measurements (Grassart et al., 2014). Surprisingly, we observed that 70% of CLC tracks co-localized with EndoA2 (Figure S3B), which favors an important role of endophilin during CME. However, EndoA2 depletion did not impact significantly the recruitment of Dnm2 during CME, and this indicates that EndoA2 is not required to recruit Dnm2. Strikingly, the recruitment of EndoA2 within CLC tracks was enhanced when Dnm2 was depleted (94% of co-localized CLC-EndoA2 tracks; Figure S3B). This result is reminiscent of the tubules decorated by endophilin in dynamin knockout (KO) cells (Ferguson et al., 2009), and it suggests that Dnm2 negatively regulates EndoA2 recruitment to CLC tracks.

Regarding CIE, we observed that 60% of IL-2R tracks were co-localized with Dnm2 (Figure S3B). Strikingly, this rate was reduced to 40% upon EndoA2 depletion (Figure S3B). This result indicates that EndoA2 is implicated in Dnm2 recruitment during CIE. In addition, we observed that Dnm2 depletion did not alter the rate of EndoA2 recruitment to IL-2R tracks (about 40% of co-localization rate in both conditions) (Figure S3B). Thus, we demonstrated that EndoA2 is a core component of CME, but its role is not essential for the recruitment of Dnm2. In contrast, EndoA2 is less frequently recruited to IL-2R internalization, but its function for recruiting Dnm2 is primordial. Overall, we conclude that EndoA2 is a universal core endocytic component shared by both endocytosis routes but exhibits different necessities for recruiting Dnm2.

Identification of Active CME and CIE Tracks by Best-Fitting Methods and Impact of Dynamin2

Since EndoA2 is strongly associated to CLC tracks, we decided to decipher more accurately its recruitment to CME and CIE track lifetimes. The lifetime of clathrin-coated structures (CCSs) is highly variable at the plasma membrane, and it was already reported to be composed of abortive and productive events (Loerke et al., 2009). Thus, it is necessary to precisely identify each of these populations to determine accurately the recruitment of EndoA2 during CME. To identify unambiguously and not based *a priori* on the different track populations, we used a statistical approach on the lifetime distributions of CLC for CME and IL-2R for CIE. Then, to identify the active population, representing efficient and dynamic endocytic events that should strongly depend on dynamin, an essential player of both CME and CIE of IL-2R, we tested concomitantly our results by comparing the distribution of the identified populations in cells depleted for Dnm2.

Statistical Classification of Heterogeneous CME Track Populations

First, we focused on the lifetimes of CLC tracks, which did not recruit EndoA2 (non-co-localized) using Hep2β-CLC-RFP^{EN}/EndoA2-GFP^{EN}. We observed that the distribution follows an exponential decay (Figure 2A). This population is mainly composed of short-lived CLC tracks at the plasma membrane. This result echoes previous studies accounting these events for aberrant detection and/or non-productive clathrin assembly at the plasma membrane (Loerke et al., 2009). Then, we analyzed CME events during which EndoA2 was co-localized (Figure 2B). The distribution of CLC-EndoA2 co-localized tracks was different from the non-co-localized ones, but part of the distribution fitted with an exponential one (Figure 2B). Thus, it is likely that this population represents the previously defined early/late abortive endocytic events (Ehrlich et al., 2004; Loerke et al., 2009). Accordingly, part of CLC-EndoA2 co-localized tracks did not show an exponential distribution (Figure 2B).

To better characterize the different CLC subpopulations, we fitted their lifetimes with a mixture model defined by the sum of an exponential distribution and N Gaussian distributions. The number of Gaussian distributions was determined statistically by the Bayesian Information Criterion (BIC), which in this case gave N equal to four (Figure S4). Therefore, we obtained the following five CLC populations (Figure 2C). The exponential distribution was named Expo and had an average of 25 s (±25 s) and accounted for 33% of tracks. The four Gaussian distributions were called Pop1, Pop2, Pop3, and Pop4. We measured that Pop1 had an average lifetime of 90 s (±40 s) and represented 35% of the tracks, Pop2 had an average lifetime of 170 s (±40 s) and represented 18% of the tracks, Pop3 had an average lifetime of 257 s (±20 s) and represented 6% of the tracks, and, finally, Pop4 had an average lifetime of 290 s (±10 s) and represented 8% of tracks (Figures 2B–2D).

To test whether our statistical method is able to retrieve the simulated populations and how performances depend on the number of tracks, we generated synthetic time-lapse sequences where the endocytosis kinetics were pre-defined as in Figures 2A–2D and tunable (Figure 3; Experimental Procedures). The results show that (1) track durations measured with eTrack were very close to simulated durations (ground truth), and this confirms the robustness of eTrack in very cluttered imaging conditions; (2) our statistical method (BIC) was particularly robust since we obtained always 4 populations when at least 2,000 tracks were analyzed (Figure 3B; in our experimental data we analyzed more than 5,000 tracks); and (3) our method also determined the mean duration of each population and their proportion very accurately (Figures 3C and 3E). The only bias that we observed in our statistical analysis was the slight over-estimation of abortive exponential tracks to the detriment of the first active population. Overall, our approach supports a classical view of CME describing distinct subpopulations composed of short-lived and long-lived endocytic events. Though, the co-integration of endocytic factor recruitment in our analysis allowed us to refine this model, exhibiting 5 different populations.

Dynamin Is Required for an Active CME Population

Since Dnm2 is an essential factor of CME, we analyzed how its depletion influences the distribution of CLC populations (Figures 2E–2H). Dnm2 was knocked down in Hep2β-CLC-RFP^{EN}/EndoA2-GFP^{EN} cells using siRNA, and similar live-cell imaging acquisitions and analysis were performed as described previously. Strikingly, the absence of Dnm2 led to 3 Gaussian populations instead of 4 in control conditions, according to the BIC value (Figure S4). This result is translated by the disappearance of one Gaussian population of CLC. The best-fitting mixture model showed that the population 1 (showing a mean lifetime

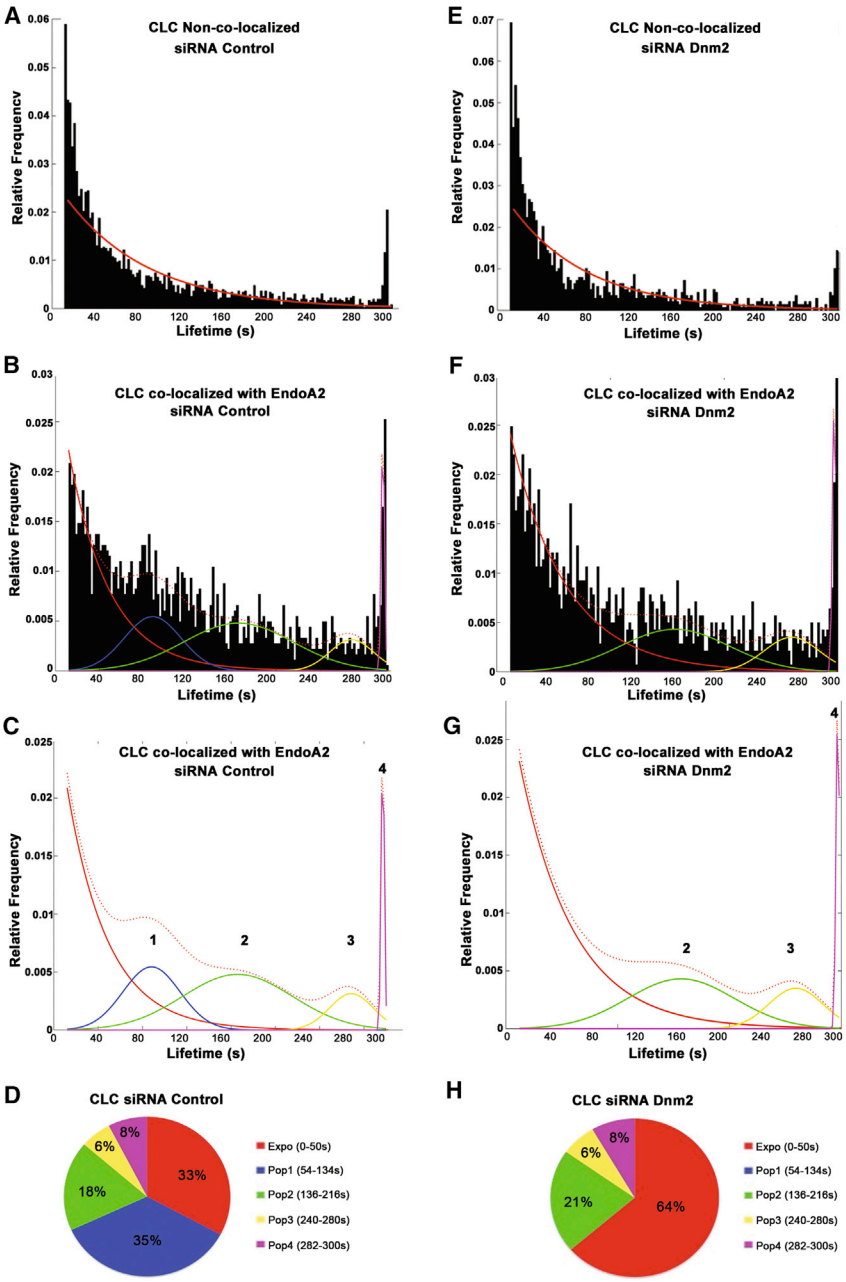

Figure 2. Classification of CLC Tracks Based on Their Lifetime Using Statistics and Fitting Methods

(A–H) Cells were imaged by TIRF microscope at 0.5 Hz for 300 s and analyzed using eTrack implemented in Icy software, as detailed in Figure S2. Lifetime is expressed in seconds, and distribution is expressed as a relative frequency of CLC tracks.

(A–D) Hep2β-CLC-RFP^{EN}-EndoA2-GFP^{EN} cells transfected with siRNA Control are shown (n = 8,405 tracks).

(E–H) Hep2β-CLC-RFP^{EN}-EndoA2-GFP^{EN} cells transfected with siRNA Dnm2 are shown (n = 4,057).

(A and E) Distribution of CLC tracks lifetimes that do not co-localize with EndoA2 in siRNA Control (A) or siRNA Dnm2 (E).

(B and F) Distribution of CLC tracks lifetimes that co-localize with EndoA2 in siRNA Control (B) or siRNA Dnm2 (F) condition. Overlay of (C) and (G) is shown.

(C and G) Identification of subpopulations of CLC tracks co-localizing with EndoA2, with best fitting of the distribution of CLC track lifetimes using a mixture model composed of an exponential and four Gaussians. These subpopulations were respectively termed expo (red), pop1 (blue), pop2 (green), pop3 (yellow), and pop4 (purple).

(D and H) Contribution of the identified subpopulations. Lifetime windows of each subpopulation are shown on the right. Results of siRNA Control (D) and siRNA Dnm2 (H) conditions are shown.

of 90 s) disappeared to the advantage of the exponential distribution (Expo, 63% of tracks; Figures 2G and 2H). The other Gaussian populations did not change their mean lifetimes or their frequency in this condition (Pop2, 21%; Pop3, 7%; and Pop4, 8% of tracks; Figures 2E–2H).

Since Dnm2 is absolutely required for the completion of CME, this result reveals population 1 as the active population of CME. In these conditions, we believe that Pop2 might represent late productive CLC tracks in which the process would be delayed. Regarding Pop3 and Pop4, which are frequently defined as non-terminal events, their characteristic static appearance (staying visible during the entire movie) does not allow us to determine their productivity based on CLC lifetime. Altogether, these data confirm that the tracking and fitting methods based on statistics gave robust results. Based on the combination of CLC dynamics and protein co-localization, our approach allows us to reveal the endocytic status defined as abortive, active, late productive, and static (non-terminal).

Statistical Classification of CIE Heterogeneous Populations

Using this methodology, we analyzed the IL-2R dynamics at the plasma membrane. Indeed, we aimed at determining the organization of CIE, which remains yet unknown. Since this pathway also requires dynamin for its completion, we used the same statistical approach as performed for CME analysis. Briefly, we analyzed and compared the distribution of IL-2R lifetimes co-localizing or not with EndoA2-GFP, in Hep2β-EndoA2-GFP cells depleted for Dnm2 or not as control cells. Interestingly, we observed that non-co-localized IL-2R tracks have a similar lifetime distribution fitting with an exponential distribution as observed in CME (Figure 4A). Thus, it is likely that these short-lived tracks represent aberrant tracks or non-productive endocytic tracks as well. In control conditions, IL-2R-EndoA2

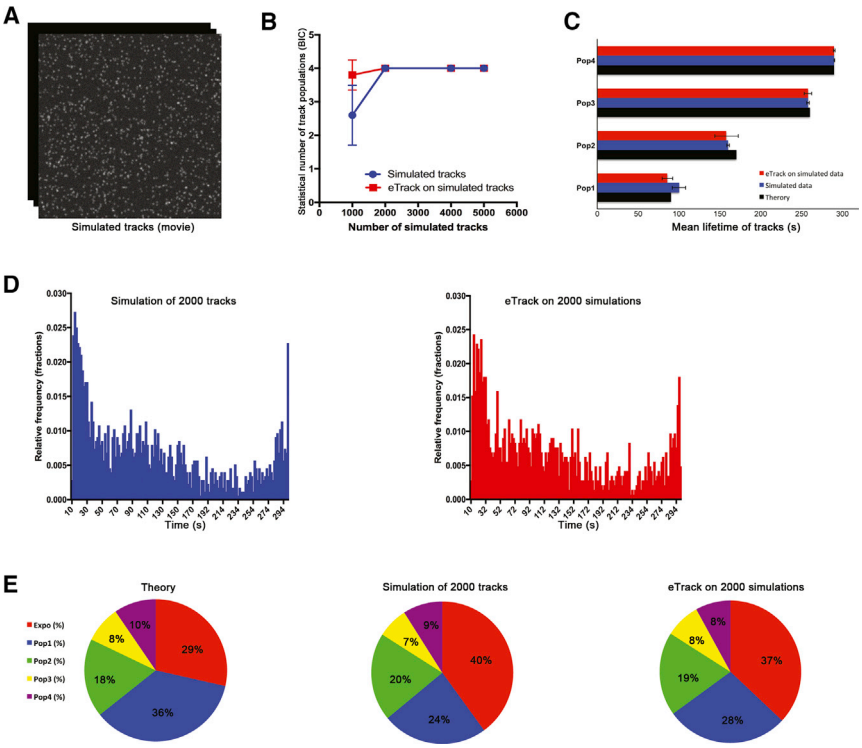

Figure 3. Testing the Robustness of Our Statistical Approach with Simulated Data

(A) Synthetic time sequences with known and tunable endocytosis kinetics are generated with the plugin EndoSim in Icy (Experimental Procedures).

(B) Statistical computation (BIC analysis) of the number of track populations for an increasing number of simulated tracks (1,000, 2,000, 4,000, and 5,000 tracks). BIC analysis was performed on the simulated track durations (ground truth, blue circles) and the durations of tracks measured with eTrack on synthetic fluorescence sequences (red squares).

(C) Mean lifetimes (±SD, 5 simulations with n = 2,000 tracks) of the different track populations (4 Gaussian populations) provided by the BIC analysis for simulated durations (blue) and tracks measured with eTrack on synthetic sequences (red). The black bar indicates the ground truth.

(D) Representative histograms of the simulated track durations and those measured with eTrack (n = 2,000 simulated tracks).

(E) Proportions of populations according to the theory, to simulated tracks, or to eTrack on simulatons (2,000 tracks).

co-localized tracks followed a different distribution that fits partly with the exponential (Figures 4A and 4B). Using the same mixture model as for CME, we performed a BIC test to identify the number of Gaussian distributions beside the exponential one, and we found 3 other populations (Figure S4). The best fitting for IL-2R lifetimes was obtained with an exponential (60% of tracks) and 3 Gaussian populations (Pop1–3): Pop1, 130 ± 30 s, 27% of tracks; Pop2, 183 ± 21s, 10% of tracks; and Pop3, 590 ± 10 s, 3% of tracks (Figures 4B–4D). While population 3 represents static tracks of IL-2R that are not internalized, the first two Gaussian populations might be the active CIE endocytic tracks.

Coherently, the depletion of Dnm2 (Hep2β-EndoA2-GFP^{EN} siRNADnm2) led to a very different distribution of IL-2R-EndoA2 co-localized tracks (Figures 4E–4H). Strikingly, in this case the BIC was 2 (Figure S4) and the fitting of these lifetime distributions with an exponential and 2 Gaussians revealed the suppression of the two first populations (Pop1 + 2, mean at 130 and 183 s, respectively) to the advantage of the exponential curve (89% of tracks) and an enrichment of the static population 3 (11% of tracks; Figure 4G-H). Thus, IL-2R active tracks are composed of 2 populations (active 1 and 2) having each 130- and 183-s mean lifetimes and both deeply affected in the absence of Dnm2. Altogether CIE tracks can be subdivided into abortive, active, and static populations. This result reinforced our statistics-based strategy to identify the active CIE endocytic tracks.

In summary, we have developed a statistical quantification of heterogeneous CME and CIE track populations. Using co-localization and depletion data, we characterized the tracks' subpopulations upon their activity. Altogether, our results indicate that both CME and CIE are highly heterogeneous. Moreover, both pathways share similar classes (abortive, active, and static events), suggesting a mechanistic conservation between endocytosis pathways in mammalian cells.

EndoA2 Depletion Impacts Only the Dynamics of CIE

To investigate how EndoA2 regulates CME and CIE dynamics, we depleted EndoA2 in genome-edited cells CLC-RFP^{EN}/Dnm2-GFP^{EN} (for CME) and Hep2β-Dnm2-GFP^{EN} (for CIE), and we analyzed whether EndoA2 contributed to the subpopulations of CLC and IL-2R tracks co-localizing or not with Dnm2. For this we adopted the same approach described in Figures 2 and 4, and we identified early abortive, active, late productive, and static subpopulations for CLC and IL-2R tracks in control and siRNA EndoA2-treated cells. In CME, the depletion of EndoA2 did not affect the distribution of the CLC lifetimes co-localized with Dnm2 (Figures 5A and 5B). Indeed, the same proportion of CLC tracks were found in early/late abortive, active, or static tracks in the presence or absence of EndoA2 (Figures 5A and 5B). This result is in agreement with the absence of impact of EndoA2 depletion on CME cargo uptake measured previously (Figure S1).

In contrast, the depletion of EndoA2 led to major changes in CIE lifetime distribution (Figures 5C and 5D). Indeed, we observed a 35% decrease of the first active population and a total disappearance of the second active population. Thus, active populations (active 1 + 2) were strongly reduced. This result is in total agreement with the strong inhibition of IL-2R uptake measured in Figure S1. Accordingly, we measured an increase of the exponential and static populations by 40% and 70%, respectively (Figures 5C and 5D). Interestingly, this result

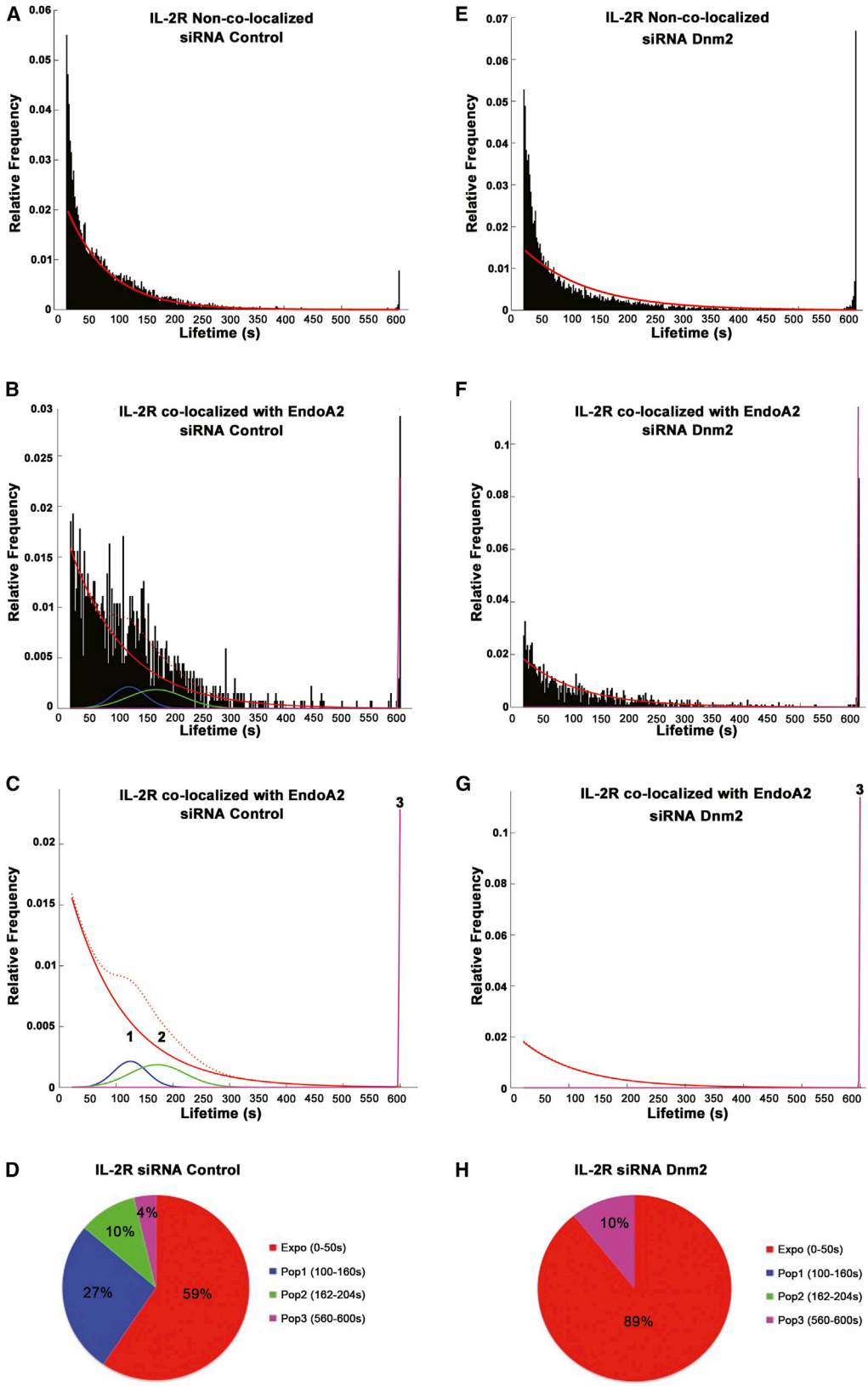

(legend on next page)

is reminiscent of the phenotype observed in Dnm2 knockdown. Thus, our results strongly favor a model in which CIE, but not CME, is highly dependent on the interplay between EndoA2 and Dnm2.

Dynamical Orchestration of Dnm2 and EndoA2 in CME and CIE

To gain a better understanding of EndoA2 interplay with Dnm2 during CME and CIE, we analyzed the duration of co-localization of each of these factors in both endocytosis pathways with respect to each CLC or IL-2R subpopulations. In addition, we also analyzed the time of departure of these proteins with respect to the termination of CLC or IL-2R endocytic events (i.e., the disappearance of CLC or IL-2R from the plasma membrane). Indeed, we hypothesized that an alteration of Dnm2 or EndoA2 duration and/or departure might reveal an operational mechanistic defect during endocytosis.

In CME, we observed a different duration of Dnm2-CLC co-localization depending on the subpopulations. In the active tracks, we observed a sharp distribution of the duration of Dnm2-CLC co-localization, showing an average time of Dnm2 interaction of about 35 s (Figure 6A; Figure S5A). This result is in agreement with previous studies (Grassart et al., 2014). Regarding long-lived CCS subpopulations (i.e., late productive and static populations), Dnm2 presented extensive duration of interaction with clathrin as compared to the active subpopulation (54 and 90 s respectively; Figure 6A; Figure S5A). On the contrary, for short-lived clathrin tracks (representing early abortive events), Dnm2 exhibited a shorter association as compared to active and long-lived CLC tracks (average duration of 16 s; Figure 6A; Figure S5A). We performed correlation studies between the duration of Dnm2 interaction and the lifetimes of CLC tracks, and we observed a good correlation (r Spearman > 0.5; Figure 6F). This result might indicate that Dnm2 is recruited until the clathrin-coated pit has reached a satisfying level of maturation, which is dependent on several key steps that vary in duration, upon the population of the CLC tracks (active, late productive, or static). In conclusion, we found that Dnm2 must fulfill a strict and precise spatiotemporal interaction within CCS to produce a complete CME event. Next, we interrogated whether EndoA2 depletion regulates Dnm2 function by measuring its time of interaction during CME. We did not observe any impact of EndoA2 on the duration of Dnm2 co-localization within the active subpopulation of CME (Figure 6A; Figure S6B). This result confirms that EndoA2 depletion does not impair Dnm2 function or CME.

Next, we investigated the lifetime of Dnm2 interaction during CIE. Surprisingly, we observed a broader distribution of Dnm2 lifetime within the CIE active subpopulation as compared to CME. However, we measured a similar average duration (about 38 s; Figure 6B; Figure S5C). This result is in agreement with a lower correlation (Figure 6F) found between Dnm2 and IL-2R lifetimes in comparison to CLC, and it suggests that the commitment of the CIE machinery for recruiting Dnm2 during CIE is less reliable as compared to CME. Though, the comparable average lifetime favors a conserved mechanistic action of Dnm2 during both endocytosis pathways. Regarding other subpopulations of IL-2R, we observed similar results as observed for CME. In particular, as observed during CME, a shorter interaction of Dnm2 was noticed during abortive tracks (mean at 14 s) and longer interaction was observed in static tracks (mean at 150 s; Figure 6B; Figure S5C). Interestingly, the depletion of EndoA2 (Hep2β-Dnm2-GFP^{EN} siRNA EndoA2) did not affect significantly the duration of Dnm2 interaction to IL-2R tracks (Figure 6B; Figure S5D). Thus, the interplay between EndoA2 and Dnm2 is essential for Dnm2 recruitment, but it does not regulate Dnm2 function. Altogether these data show that Dnm2 recruitment during CME is more precisely and securely regulated compared to CIE, during which Dnm2 recruitment is strongly dependent on EndoA2.

Lastly, we analyzed the duration of EndoA2 during CME and CIE. Irrespective of the endocytosis mechanisms, we observed a similar distribution of the duration of EndoA2 within CLC or IL-2R subpopulations. We measured an average duration of EndoA2 of about 30 s (±10 s) in both pathways (Figures 6C and 6D; Figure S6). As expected, the duration of EndoA2 interaction in abortive events was shorter with an average lifetime of about 15 s (±5 s). Interestingly, analysis of late productive and static subpopulations revealed a limited increase in the duration of EndoA2 interaction in both CME and CIE. Correlation studies showed a low correlation between the duration of endophilin interaction and CLC/IL-2R lifetimes (r = 0.3; Figure 6F). This suggests that the recruitment of endophilin in CME and CIE is timely constrainted and/or stochastic. As compared to Dnm2 duration, this result suggests an even greater conservation of EndoA2 function between these two endocytosis routes. While depletion of Dnm2 abolished the active subpopulations in both endocytic pathways, we measured a prolongation of EndoA2 interaction within CLC and IL-2R tracks in both static and late productive subpopulations of CME and CIE, as compared to control conditions (Figures 6C and 6D; Figures S6B and S6D). Especially for CME, the duration of co-localized

Figure 4. Classification of IL-2R Tracks Based on Their Lifetime Using Statistics and Fitting Methods

(A–H) Cells were imaged by TIRF microscope at 0.5 Hz for 600 s and analyzed using eTrack implemented in Icy software as detailed in Figure 2. Lifetime is expressed in seconds, and distribution is expressed as a relative frequency of IL-2R tracks.

(A–D) Hep2β-EndoA2-GFP^{EN} cells transfected with siRNA Control are shown (n = 14,658 tracks).

(E–H) Hep2β-EndoA2-GFP^{EN} cells transfected with siRNA Dnm2 are shown (n = 15,217).

(A and E) Distribution of IL-2R track lifetimes that do not co-localize with EndoA2 in siRNA Control (A) or siRNA Dnm2 (E).

(B and F) Distribution of IL-2R track lifetimes that co-localize with EndoA2 in siRNA Control (B) or siRNA Dnm2 (F) condition. Overlay of (C) and (G) is shown.

(C and G) Identification of subpopulations of IL-2R tracks co-localizing with EndoA2, with best fitting of the distribution of CLC track lifetimes using a mixture model composed of an exponential and three Gaussians. These subpopulations were respectively termed expo (red), pop1 (blue), pop2 (green), and pop3 (purple).

(D and H) Contribution of the identified subpopulations. Lifetime windows of each subpopulation are shown on the right. Results of siRNA Control (D) and siRNA Dnm2 (H) conditions are shown.

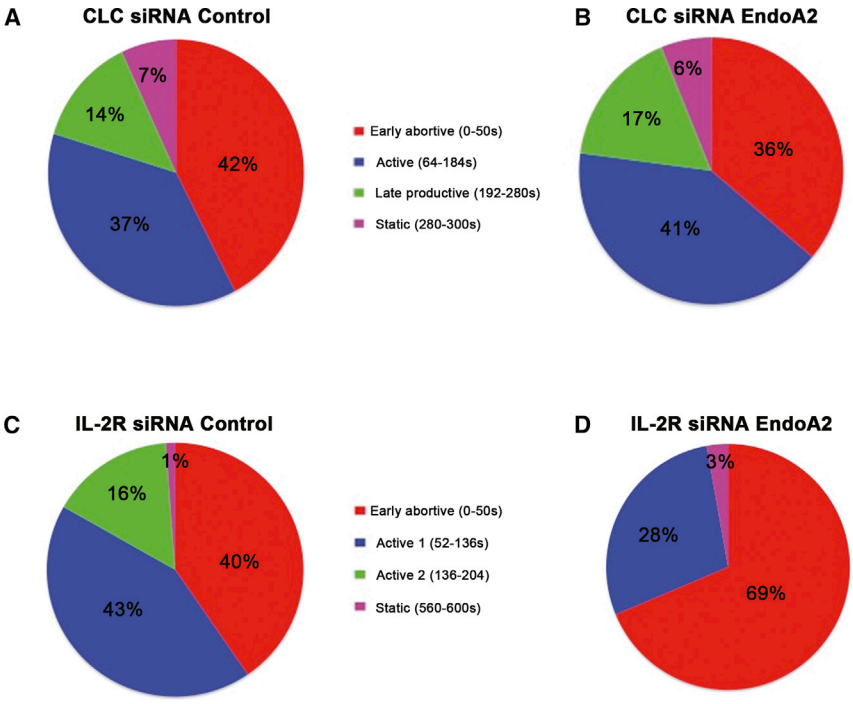

Figure 5. Effect of EndoA2 Depletion on Lifetime Distribution of CLC and IL-2R

(A and B) Distribution of the subpopulations of CLC tracks (n > 9,400), as described in Figure 2, in SK-MEL-2 CLC-RFP^{EN}/DNM2-GFP^{EN} cells depleted of EndoA2 (B) or not (A).

(C and D) Distribution of the subpopulations of IL-2R tracks (n > 7,050), as described in Figure 4, in Hep2β-DNM2-GFP^{EN} cells depleted of EndoA2 (D) or not (C).

EndoA2 within CLC tracks doubled upon Dnm2 depletion (Figure 6C). This result is in agreement with the increase of CLC-EndoA2 co-localization (Figure S3) and a higher correlation between EndoA2 and CLC lifetimes (r = 0.48) (Figure 6F) in the absence of Dnm2.

Overall, our analysis reveals three major features on Dnm2-EndoA2 regulation. First, Dnm2 and EndoA2 have similar and defined durations in both endocytosis pathways (about 30 s), which reinforces the hypothesis on the interplay between these factors. Second, our data highlight the fine-tuning of Dnm2 recruitment within static endocytic sites, which is translated by longer Dnm2 interaction. This behavior was not observed for EndoA2 (or at least much more contained), which suggests that EndoA2 uncoupled its function from Dnm2 at some point. Finally, we observed that Dnm2 unleashed the duration of EndoA2 interaction to CME and CIE. We propose that Dnm2 acts as a master switch for EndoA2 during endocytosis.

Dnm2 Regulates EndoA2 Departure

To better characterize the function of Dnm2 and EndoA2, we interrogated how dynamin interplay with EndoA2 controls the timing of EndoA2 departure during CME and CIE. To do so, we analyzed the time of interaction of each protein (Dnm2 and EndoA2) in proportion to the lifetime of the endocytic event (CLC or IL-2R). This method allowed us to determine the moment of Dnm2 and EndoA2 departure for each single endocytic event (Figure 6E). We observed that Dnm2 and EndoA2 stayed mainly until the end of CLC or IL-2R tracks in any cellular conditions (departure at 85%–100% of the track lifetimes in siRNA Control, EndoA2, or Dnm2; Figure S7). More precisely, the final times of interaction of Dnm2 and EndoA2 were occurring at 98% and 89% of CLC active tracks, respectively (Figure 6E). Coherently to our previous result (Figures 6A–6D), Dnm2 depletion increased the final time of interaction of EndoA2 that was at 96% of CLC tracks in this condition. For CIE, we observed that Dnm2 and EndoA2 were leaving sooner at 86% and 76%, respectively, of IL-2R active tracks. Again, Dnm2 depletion increased the final time of EndoA2 that was leaving at 82% of IL-2R static tracks (Figure 6E). This shows that Dnm2 regulates the departure of EndoA2 in both CME and CIE. Altogether our results demonstrate the interplay of EndoA2 and Dnm2 that is acting at the end of both CME and CIE processes.

Stoichiometry of Dnm2 and EndoA2 during CME and CIE

Finally, to better understand the interplay between Dnm2 and EndoA2, we explored the stoichiometry of both proteins during endocytosis events in living cells, and we interrogated the consequence of a perturbation of Dnm2/EndoA2 concentration on each other. Recently, we and others have demonstrated that expression of fluorescent fusion proteins expressed from their native promoters enables estimation of the number of molecules in living cells (Cocucci et al., 2014; Grassart et al., 2014). Briefly, purified EGFP molecules were seeded on a cleaned coverslip at a low density and imaged (Figures 7A–7D). Using such calibrated imaging systems and intensity standard, we determined that about 28.4 molecules of Dnm2 (±7.4 molecules) are recruited at its peak of recruitment during CME (Figure 7E). This result is similar to previous results obtained in another cell line background, and it indicates a conserved action of Dnm2 during CME. Interestingly, we found a small but significant reduction of Dnm2 molecule recruitment during CIE, with an average of 23.2 Dnm2 molecules (±8.6 molecules) (Figure 7E). Such counts suggest that Dnm2 is barely able to produce a short helix during CIE. Thus, it appears that CIE needs less Dnm2 than CME to pinch off the vesicle.

Then, we interrogated the accumulation of EndoA2 in each of these endocytosis pathways. We found that about 15.22 (±5.4 molecules) and 14.02 (±5.1 molecules) molecules of EndoA2 were recruited during CME and CIE, respectively (Figure 7F). While subtle differences exist in the composition of both machineries, our results reveal a conserved stoichiometry (about 2:1) for the couple Dnm2:EndoA2 during both mechanisms of

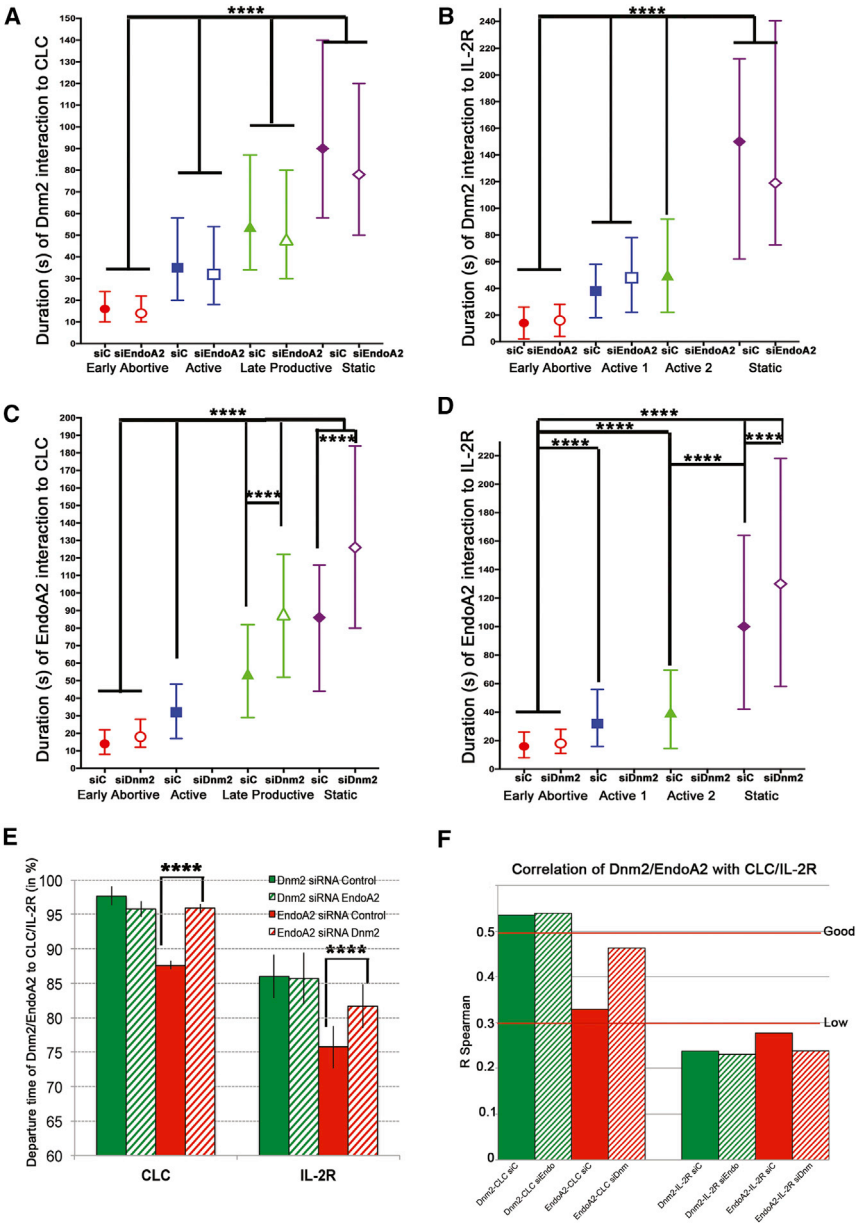

Figure 6. Average of Duration of Co-localization and Final Time of Interaction of Dnm2 or EndoA2 with CLC or IL-2R Tracks

(A–D) Average duration of co-localization per subpopulations for each condition: siRNA control (filled symbols) and siRNA Dnm2 or EndoA2 (open symbols). (A) Dnm2-CLC co-localized tracks (mean ± SD, 350 < n < 2,000), (B) Dnm2-IL-2R co-localized tracks (mean ± SD, 50 < n < 1,000), (C) EndoA2-CLC co-localized tracks (mean ± SD, 280 < n < 1,500), and (D) EndoA2-IL-2R co-localized tracks (mean ± SD, 87 < n < 1,900) are shown. Results are expressed in seconds.

(E) Average time of departure of Dnm2 or EndoA2 proteins with CLC or IL-2R tacks (n > 900 tracks ± SD, except for siRNA Dnm2 n > 232). Analysis was proportionally completed with respect to the extent of the CLC and IL-2R track. Results are expressed as a percentage of each track duration. Unpaired t test, ****p < 0.001.

(F) Correlation analysis using r Spearman linking the duration of EndoA2/Dnm2 interaction to either CLC or IL-2R lifetimes in siRNA control (siC) or siRNA EndoA2/Dnm2 (siEndo/siDnm) condition.

endocytosis. Since CME and CIE lifetimes are heterogeneous, we then sought to analyze Dnm2 and EndoA2 concentration (at its peak recruitment) depending on the lifetime of CME and CIE events. We did not observe any correlation between Dnm2 concentration and the lifetime of CME and CIE (Figures 7G and 7H). This high stability probably reflects the formation of a stable Dnm2 ring during the last stage. Interestingly, we observed that the number of molecules of EndoA2 is correlated with the lifetime of CLC, but not with IL-2R (r about 0.5) (Figures 7I and 7J). Thus, only CME adapts locally the EndoA2 concentration. Finally, we assessed the impact of a lower concentration of Dnm2/EndoA2 on its relative partner during CME and CIE. We observed that the depletion of EndoA2 does not exhibit any impact on the maximum number of molecules recruited of Dnm2 during CME and CIE (Figure 7K). On the other hand, we observed that Dnm2 depletion induces a large increase of EndoA2 concentration in CME, but not in CIE (Figure 7L). Thus, the remodeling capacity between CME and CIE machinery is different.

DISCUSSION

We presented a comprehensive study of EndoA2 dynamics and function within CME and CIE. This work settles EndoA2 as a conserved endocytic partner in both endocytosis pathways. While EndoA2 is robustly recruited during the last stage in both CME and CIE mechanisms, we found that its absence impaired Dnm2 initial recruitment only during CIE. By analyzing protein stoichiometry during endocytosis, our results show that Dnm2:EndoA2 stoichiometry (about 2:1) is conserved between the two endocytosis routes. While a reduction of EndoA2 concentration has little impact on the stoichiometry of its partner in CME and CIE, the depletion of Dnm2 increases the number of EndoA2 only in CME. Overall our study refines the critical contribution of endophilin in CIE.

Dnm2 and EndoA2 in CME versus CIE

Strong similarities have been observed in the temporal organization and stoichiometry of Dnm2 and EndoA2 between both endocytosis pathways. Our findings reinforce a two-step model of CME: (1) a maturation step during which dynamin participates in the control of the CCP maturation; and (2) once sufficient maturation of the endocytic site is accomplished, an irreversible quanta

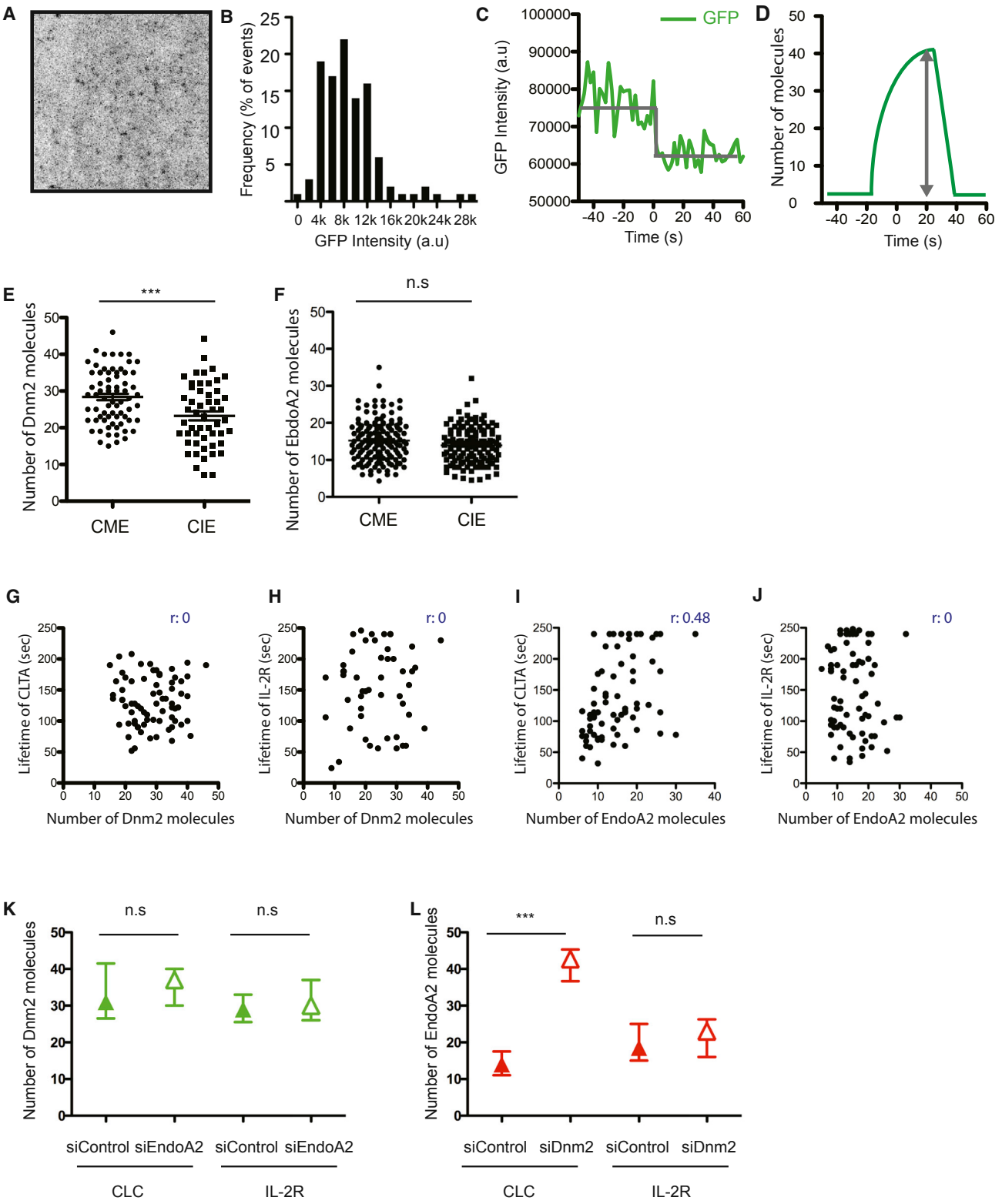

Figure 7. Quantification of EndoA2 and Dnm2 Recruitment during CME and CIE

(A) Representative image from a time series of EGFP proteins deposited on a glass coverslip illuminated using TIRF microscopy. Spots represent EGFP molecules. Picture shown has been enhanced using a time projection of 5 consecutive frames.

(legend continued on next page)

of Dnm2 molecules is ultimately recruited to proceed to the vesicle scission. Interestingly, we found that the number of EndoA2 molecules and its time of interaction is slightly correlated to CCP lifetime, but not with IL-2R. This finding probably suggests that CME machinery is more able than CIE to finely modulate EndoA2 concentration upon its maturation constraints and/or recruitment of dynamin. Regarding CIE, we noticed that Dnm2 has a less precise timing of recruitment and duration of action than CME. Since CIE recruits slightly less Dnm2 molecules than CME, it is possible that the CIE machinery needs a prolonged interaction to fulfill the scission process as compared to CME.

Strikingly, our work points out that EndoA2 is required for the efficient recruitment of Dnm2 to IL-2R active tracks in contrast to CME. This last result is in total agreement with the fact that endophilin is dispensable for CME, but not for CIE (Figure S1) (Boucrot et al., 2015; Renard et al., 2015). Unexpectedly, we observed that EndoA2 is recruited within 70% of active CME events, whereas this rate dropped to 36% for IL-2R in CIE. In addition, we observed that the maximum number of endophilin is similar between CIE and CME. Since EndoA2 is critical for CIE cargo uptake only, these puzzling results might reflect that IL-2R endocytic machinery is not as robust and regulated as CME. Altogether these results reinforce the hypothesis of a relatively inefficient process. Several other reasons could explain these differences between CME and CIE. First, the redundancy of accessory proteins in CME might provide additional capacity to recruit dynamin through other protein interactions without changing its final stoichiometry. This level of redundancy could also explain the dependence of EndoA2 for the initial recruitment of Dnm2 (but not in its scission activity) in CIE only. Other BAR domain proteins have been associated in CME. Amphiphysin/BIN1 is the closest counterpart of endophilin involved during CME. Recently, an *in vitro* study proposed that both proteins cooperate to recruit Dnm2 to clathrin-coated pits (Meinecke et al., 2013). To date, endophilins are the only BAR domain proteins involved during CIE of IL-2R. Besides the redundancy of BAR domain proteins, physical constraints, such as membrane curvature and neck thickness, might differ between these two endocytic routes. For example, the assembly of clathrin coat might provide enough tension to promote an efficient thickness of the neck, more prone to scission. This hypothesis could explain the extension of EndoA2 molecules upon Dnm2 depletion in CME only. Determining the precise spatiotemporal organization of these proteins relative to the shape of the membrane and architectural structure of these endocytosis events might be an invaluable insight to better understand CIE.

Advanced Analytics of CME and CIE Dynamics

Use of genome-edited cells leads to much dimmer molecule spots, which might hinder the robust tracking of endocytic events (Aguet et al., 2013). Moreover, analysis of unstructured data (i.e., without a pre-defined data model) is currently a challenge for interpreting the extensive amount of data generated by automatic tracking of single endocytic events from live-cell imaging. In the present study, we developed a framework combining a global tracking method that fully exploits confinement of endocytosis and statistical classification of heterogeneous track populations. This approach allowed us to: (1) identify the heterogeneous nature of CIE and CME, and (2) reveal the active population of these two endocytosis mechanisms. To date, few studies have performed such quantitative approaches to evaluate CME dynamics and none has been performed for CIE, to the best of our knowledge.

Recently, Aguet et al. (2013) proposed another approach called Master-Slave to study CME. This method relies on a Master channel, which determines endocytosis sites by tracking a bright, robust, and permanent marker. Using this position, a dimmer molecule of interest can be robustly tracked along the followed Master. Unfortunately, the absence of coat protein circumvents such an approach for studying CIE. Furthermore, overexpression refashions the native stoichiometry, which might adverse the questioned cellular process. Finally, this approach uses a fluorescent channel for Master tracking that could be exploited for exploring multiple molecule interaction instead. Here, our algorithm relies on the constraint displacement of endocytic events to identify active events. The benefit of a lowered dependency on signal intensity is exemplified by the exclusive use of endocytic protein expressed under their native regulation. Nevertheless, our analysis using a robust automated tracking method and statistical classification is close to the approach described in Loerke et al. (2009). However, our model to classify tracks by statistics is different since it generates more subclasses of the CME and CIE tracks, allowing precision of their kinetics. Moreover, the advantage of our study is the comparative analysis of the track lifetime classification in the absence and presence of dynamin, an essential factor of CME and CIE. This method allowed us to identify active tracks for both CME and CIE processes that represent authentic endocytic events.

Organization of Endocytosis

Previously, Loerke et al. (2009) identified three major subpopulations in CME: early abortive, late abortive, and productive events. While our results agree with the functional assignment

(B) Distribution of EGFP intensity measured (n = 107).
(C) Representative fluorescence intensity trace corresponding to a single bleaching step of an EGFP molecule.
(D) Schematic representation of the maximum number of molecules counted during endocytosis.
(E) Distribution of the maximum number of Dnm2-GFP molecules recruited during CME or CIE events (mean ± SEM; n = 72 for CME and n = 52 for CIE).
(F) Distribution of the maximum number of EndoA2-GFP molecules recruited during CME or CIE events (n = 144 for CME and n = 133 for CIE).
(G and H) Dot plot of the maximum number of Dnm2 molecules relative to CLTA lifetime (n = 72) (G) or IL-2R lifetime (n = 52) (H).
(I and J) Dot plot of the maximum number of EndoA2 molecules relative to CLTA (n = 72) (I) or IL-2R lifetime (n = 82) (J). Each dot represents a single endocytic event.
(K) Distribution of the maximum number of Dnm2-GFP molecules recruited during CME or CIE events in EndoA2-depleted cells (filled triangle) or in control condition (open triangle) (n = 17, 19, 37, and 37).
(L) Distribution of the maximum number of EndoA2-GFP molecules recruited during CME or CIE events in Dnm2-depleted cells (filled triangle) or in control condition (open triangle) (n = 33, 36, 28, and 30).

of abortive versus productive events, our analysis revealed subtle differences. Here, a single abortive subpopulation and at least three productive subpopulations of CCS were identified in CME. These different signatures might be explained by the analytics design of each study. Moreover, the use of different cell lines might also account for some of the observed differences. Indeed, we used human SK-MEL-2 and Hep2β cells (Doyon et al., 2011; Grassart et al., 2014), while Loerke et al. (2009) used primate BSC-1 cell line, a model exhibiting rarely so-called static or non-terminal events. Anyhow, both analyses conclude on the existence of a checkpoint/restriction point controlled by the GTPase Dnm2 in CME.

Based on these results, we interrogated CIE organization. Like CME, both abortive and productive event categories were identified in CIE. Thus, our results strongly support a conserved organizational model of endocytosis regulated by Dnm2 between CME and CIE. Interestingly, many of the CIE events were identified as abortive. While some of these events might be contributed by visitors entering the evanescent field of illumination as observed during CME (Hong et al., 2015), we think that these events represent a minor contamination, if any, in CIE. Indeed, we limited such intracellular contaminations using a rapid and direct extracellular labeling against IL-2R. Since extensive washes removed almost all residual antibodies on the coverslip, it is also unlikely that the few remaining unbound antibodies constitute the majority of the plasma membrane. Second, we observed that Dnm2 depletion led to an important increase of the abortive population (up to 90%). Contaminants are unrelated and would remain insensitive to dynamin depletion. Thus, our data strongly support a genuine mechanistic clue, and we conclude that stabilization of the initial steps is critical for CIE. Since no coat protein and adaptors have been identified for IL-2R endocytosis yet, the timing and conditions favoring the initiation and maturation of CIE might be more difficult to fulfill as compared to CME, and they might explain the higher rate of abortive events. Finally, this model is reinforced by biochemical cargo uptake measuring slower kinetics of IL-2R (CIE) as compared to Tf (CME) (Basquin et al., 2013). Based on these conclusions, it will be important in the future to determine which physical and biochemical factors coordinate and control the progression of CIE.

Native Dynamics of EndophilinA in CME and CIE

To date, our understanding of endophilin dynamics relied on overexpression of the neuronal isoform endophilinA1 or the ubiquitous isoform EndoA2. Unfortunately, accumulating evidence suggests that overexpression of either isoform induces artifactual structures in the cell. This lack of specificity also restrained our evaluation of endophilins during endocytosis events. For example, a global protein survey measured a recruitment of EndoA2 in only about 20% of CME events (Taylor et al., 2011). The meaning of this low level of recruitment was unclear, and it remained debated whether it corresponded to the existence of CCS subset classes or to technical issues, such as a low signal-to-noise ratio due to overexpression. However, the recent result showing a prominent role of endophilin in CIE in contrast to CME (Boucrot et al., 2015; Renard et al., 2015) and a low co-localization level between EndoA2 and clathrin led Boucrot et al. (2015) to propose that endophilin could be used as a specific marker of CIE.

Here we addressed EndoA2 recruitment in both CME and CIE mechanisms using a genome-engineering approach to knock in GFP at the EndoA2 locus. Thus, the native dynamics of EndoA2 were followed and analyzed. We observed a robust recruitment of EndoA2 in most CME events, and we conclude that EndoA2 is an integral component of the CME machinery. Since EndoA2 is strongly associated with both CME and CIE pathways, endophilin cannot be a marker of CIE only. We believe that these differences with previous reports stem from the transient nature of EndoA2 during CME. However, we acknowledge that gene-edited versions of CLC-RFP^{EN}, Dnm2-GFP^{EN}, and EndoA2-GFP^{EN} described in this study might not behave exactly the same way as the endogenous proteins, due to the tagging of fluorescent protein; but, this approach generates the closest physiological tools allowing the study of endocytic factors recruitment in real time. In addition, IL-2R cargo was used as one bona fide marker of CIE, but we acknowledge that this might not reflect the full diversity of CIE pathways since some were reported as dynamin and/or endophilin dispensable (Renard et al., 2015).

EXPERIMENTAL PROCEDURES

Statistical Analysis of CME and CIE Endocytic Tracks

In the CLC datasets, we eliminated all the tracks with length smaller than 290 s and either starting at 1 s or ending at 300 s. Similarly, in the IL-2R datasets, we eliminated all the tracks with length smaller than 580 s and either starting at 1 s or ending at 600 s. Moreover, in all datasets of co-localized tracks, we also eliminated all the tracks with co-localization duration with the protein equal to 1 s.

After these modifications, the number of data in each dataset is, on average, divided in half (from 20,000 to 10,000 for the IL-2R datasets and from 10,000 to 5,000 for the CLC datasets).

In the following, we describe the statistical analysis for the CLC datasets. The same approach has been used for the IL-2R dataset. The CLC-siRNA Control-non-co-localized dataset follows an exponential distribution,

$$Exp(x,\lambda) = \lambda e^{-\lambda x}.$$

To define different CLC populations, we fit the dataset with the following mixture model:

$$F(x,\theta) = p_0\, Exp(x,\lambda) + \sum_{i=1}^{N} p_i\, \mathcal{N}(x,\mu_i,\sigma_i), \qquad \sum_{i=0}^{N} p_i = 1,$$

where $\mathcal{N}(x,\mu_i,\sigma_i) = (1/\sigma_i\sqrt{2\pi})e^{-((x-\mu_i)^2/2\sigma_i^2)}$ represents the Gaussian distribution corresponding to the i-th population and

$$\theta = \left(\lambda, p_0, \mu_1, \sigma_1, p_1, \ldots, \mu_N, \sigma_N, p_N\right)$$

denotes the set of parameters of the model. The (3N + 1) parameters are estimated by the maximizing the likelihood function via the expectation-maximization algorithm. The number of Gaussian distributions is chosen by performing the BIC (Figure S4), which selects the model that maximizes the likelihood by minimizing the number of parameters involved in the model. The BIC function is minimized by N = 4, which means that we can define 4 Gaussian populations for the lifetimes of CLC-EndoA2-co-localized siRNA Control tracks. We provide this statistical analysis in our Supplemental Experimental Procedures in a MATLAB script.

Generating Synthetic Time-Lapse Data

To test the robustness of our tracking (eTrack) and statistical analysis (BIC), we generated synthetic time-lapse TIRF sequences where the imaging

parameters (signal-to-noise ratio, length, spots' density) and the kinetics of endocytic tracks (number and proportion of Gaussian populations, mean duration, and SD of each track population) are known and tunable. We can therefore test how our method is close to ground truth in different conditions. Here we mimicked the CLC conditions, which are the most challenging from a statistical point of view due to the large number of track populations.

We generated synthetic 512 × 512 sequences with 150 frames and an increasing number of tracks (1,000, 2,000,...5,000). Image noise was generated with a mixed Poisson-Gaussian model (Chenouard, 2010) and the signal-to-noise ratio (SNR) adjusted to 4 (moderately noisy conditions similar to experimental movies). To simulate the motion of the cell membrane under the TIRF objective, we varied uniformly the intensity of single fluorescent spots between frames, and also we simulated a confined Gaussian motion with a zero mean and unit pixel SD per frame. Kinetics parameters of simulated track populations were as follows: Exponential (40%, mean = 12 frames [24 s]), Gaussian 1 (30%, mean = 45 frames, SD = 20 frames), Gaussian 2 (15%, mean = 85 frames, SD = 20 frames), Gaussian 3 (7%, mean = 130 frames, SD = 10 frames), and Gaussian 4 (8%, mean = 145 frames, SD = 5 frames). The endocytosis simulator is publicly available in Icy (Plugin EndoSim).

Further details can be found in the Supplemental Experimental Procedures.

SUPPLEMENTAL INFORMATION

Supplemental Information includes Supplemental Experimental Procedures, seven figures, and seven movies and can be found with this article online at https://doi.org/10.1016/j.celrep.2018.01.039.

ACKNOWLEDGMENTS

The authors would like to thank P.H. Commere from the flow cytometry facility of Institut Pasteur for the help and support with single-cell sorting. We also gratefully acknowledge S. Dallongeville and V. Meas-Yedid (Institut Pasteur) for debugging and A. Saffarian and V. Malardé (Institut Pasteur) for technical support. We thank D. Drubin for generously sharing reagents. We also thank M. Anderson, M. Ferrari, and P. Sansonetti for comments on the manuscript and support. T.L. and A.G. were supported by a Roux Fellowship from Institut Pasteur and T.L. partially supported by LABEX IBEID (ANR-10-LABX-62-IBEID). This is in part supported by an ANR grant to J.-C.O.-M. (ANR-10-INBS-04-06 France-BioImaging). L.B. was funded by the University Paris Sud/Saclay, ED SDSV.

AUTHOR CONTRIBUTIONS

L.B. performed experiments. A.G. designed, performed, and analyzed experiments (crispR and stoichiometry) and co-wrote the manuscript. T.L. designed image analysis, developed plugins (eTrack and EndoSim), performed the statistical analysis of synthetic data, and co-wrote the manuscript. G.N. designed statistical analysis and developed MATLAB scripts. C.B. performed the initial observation of Figure S1. J.-C.O.-M. supervised the work of T.L. and G.N. and performed funding acquisition. N.S. supervised the study; designed, analyzed, and evaluated data; and co-wrote the manuscript.

DECLARATION OF INTERESTS

The authors declare no competing interests.

Received: June 30, 2017
Revised: January 3, 2018
Accepted: January 12, 2018
Published: February 6, 2018

REFERENCES

Aguet, F., Antonescu, C.N., Mettlen, M., Schmid, S.L., and Danuser, G. (2013). Advances in analysis of low signal-to-noise images link dynamin and AP2 to the functions of an endocytic checkpoint. Dev. Cell *26*, 279–291.

Antonny, B. (2006). Membrane deformation by protein coats. Curr. Opin. Cell Biol. *18*, 386–394.

Antonny, B., Burd, C., De Camilli, P., Chen, E., Daumke, O., Faelber, K., Ford, M., Frolov, V.A., Frost, A., Hinshaw, J.E., et al. (2016). Membrane fission by dynamin: what we know and what we need to know. EMBO J. *35*, 2270–2284.

Basquin, C., Malardé, V., Mellor, P., Anderson, D.H., Meas-Yedid, V., Olivo-Marin, J.-C., Dautry-Varsat, A., and Sauvonnet, N. (2013). The signalling factor PI3K is a specific regulator of the clathrin-independent dynamin-dependent endocytosis of IL-2 receptors. J. Cell Sci. *126*, 1099–1108.

Basquin, C., Trichet, M., Vihinen, H., Malardé, V., Lagache, T., Ripoll, L., Jokitalo, E., Olivo-Marin, J.-C., Gautreau, A., and Sauvonnet, N. (2015). Membrane protrusion powers clathrin-independent endocytosis of interleukin-2 receptor. EMBO J. *34*, 2147–2161.

Boucrot, E., Ferreira, A.P.A., Almeida-Souza, L., Debard, S., Vallis, Y., Howard, G., Bertot, L., Sauvonnet, N., and McMahon, H.T. (2015). Endophilin marks and controls a clathrin-independent endocytic pathway. Nature *517*, 460–465.

Chenouard, N. (2010). Avancées en suivi probabiliste de particules pour l'imagerie biologique. Doctoral dissertation (Télécom ParisTech).

Chenouard, N., Smal, I., de Chaumont, F., Maška, M., Sbalzarini, I.F., Gong, Y., Cardinale, J., Carthel, C., Coraluppi, S., Winter, M., et al. (2014). Objective comparison of particle tracking methods. Nat. Methods *11*, 281–289.

Cocucci, E., Gaudin, R., and Kirchhausen, T. (2014). Dynamin recruitment and membrane scission at the neck of a clathrin-coated pit. Mol. Biol. Cell *25*, 3595–3609.

de Chaumont, F., Dallongeville, S., Chenouard, N., Hervé, N., Pop, S., Provoost, T., Meas-Yedid, V., Pankajakshan, P., Lecomte, T., Le Montagner, Y., et al. (2012). Icy: an open bioimage informatics platform for extended reproducible research. Nat. Methods *9*, 690–696.

Doyon, J.B., Zeitler, B., Cheng, J., Cheng, A.T., Cherone, J.M., Santiago, Y., Lee, A.H., Vo, T.D., Doyon, Y., Miller, J.C., et al. (2011). Rapid and efficient clathrin-mediated endocytosis revealed in genome-edited mammalian cells. Nature Cell Biology *13*, 331–337.

Ehrlich, M., Boll, W., Van Oijen, A., Hariharan, R., Chandran, K., Nibert, M.L., and Kirchhausen, T. (2004). Endocytosis by random initiation and stabilization of clathrin-coated pits. Cell *118*, 591–605.

Farsad, K., Ringstad, N., Takei, K., Floyd, S.R., Rose, K., and De Camilli, P. (2001). Generation of high curvature membranes mediated by direct endophilin bilayer interactions. J. Cell Biol. *155*, 193–200.

Ferguson, S.M., Raimondi, A., Paradise, S., Shen, H., Mesaki, K., Ferguson, A., Destaing, O., Ko, G., Takasaki, J., Cremona, O., et al. (2009). Coordinated actions of actin and BAR proteins upstream of dynamin at endocytic clathrin-coated pits. Dev. Cell *17*, 811–822.

Frost, A., Unger, V.M., and De Camilli, P. (2009). The BAR domain superfamily: membrane-molding macromolecules. Cell *137*, 191–196.

Grassart, A., Dujeancourt, A., Lazarow, P.B., Dautry-Varsat, A., and Sauvonnet, N. (2008). Clathrin-independent endocytosis used by the IL-2 receptor is regulated by Rac1, Pak1 and Pak2. EMBO Rep. *9*, 356–362.

Grassart, A., Meas-Yedid, V., Dufour, A., Olivo-Marin, J.-C., Dautry-Varsat, A., and Sauvonnet, N. (2010). Pak1 phosphorylation enhances cortactin-N-WASP interaction in clathrin-caveolin-independent endocytosis. Traffic *11*, 1079–1091.

Grassart, A., Cheng, A.T., Hong, S.H., Zhang, F., Zenzer, N., Feng, Y., Briner, D.M., Davis, G.D., Malkov, D., and Drubin, D.G. (2014). Actin and dynamin2 dynamics and interplay during clathrin-mediated endocytosis. J. Cell Biol. *205*, 721–735.

Hémar, A., Subtil, A., Lieb, M., Morelon, E., Hellio, R., and Dautry-Varsat, A. (1995). Endocytosis of interleukin 2 receptors in human T lymphocytes: distinct intracellular localization and fate of the receptor alpha, beta, and gamma chains. J. Cell Biol. *129*, 55–64.

Hohendahl, A., Talledge, N., Galli, V., Shen, P.S., Humbert, F., De Camilli, P., Frost, A., and Roux, A. (2017). Structural inhibition of dynamin-mediated membrane fission by endophilin. eLife *6*, 2270.

Hong, S.H., Cortesio, C.L., and Drubin, D.G. (2015). Machine-Learning-Based Analysis in Genome-Edited Cells Reveals the Efficiency of Clathrin-Mediated Endocytosis. Cell Rep. *12*, 2121–2130.

Lagache, T., Sauvonnet, N., Danglot, L., and Olivo-Marin, J.-C. (2015). Statistical analysis of molecule colocalization in bioimaging. Cytometry A *87*, 568–579.

Lamaze, C., Dujeancourt, A., Baba, T., Lo, C.G., Benmerah, A., and Dautry-Varsat, A. (2001). Interleukin 2 receptors and detergent-resistant membrane domains define a clathrin-independent endocytic pathway. Mol. Cell *7*, 661–671.

Loerke, D., Mettlen, M., Yarar, D., Jaqaman, K., Jaqaman, H., Danuser, G., and Schmid, S.L. (2009). Cargo and dynamin regulate clathrin-coated pit maturation. PLoS Biol. *7*, e57.

Meinecke, M., Boucrot, E., Camdere, G., Hon, W.-C., Mittal, R., and McMahon, H.T. (2013). Cooperative recruitment of dynamin and BIN/amphiphysin/Rvs (BAR) domain-containing proteins leads to GTP-dependent membrane scission. J. Biol. Chem. *288*, 6651–6661.

Milosevic, I., Giovedi, S., Lou, X., Raimondi, A., Collesi, C., Shen, H., Paradise, S., O'Toole, E., Ferguson, S., Cremona, O., and De Camilli, P. (2011). Recruitment of endophilin to clathrin-coated pit necks is required for efficient vesicle uncoating after fission. Neuron *72*, 587–601.

Perera, R.M., Zoncu, R., Lucast, L., De Camilli, P., and Toomre, D. (2006). Two synaptojanin 1 isoforms are recruited to clathrin-coated pits at different stages. Proc. Natl. Acad. Sci. USA *103*, 19332–19337.

Renard, H.-F., Simunovic, M., Lemière, J., Boucrot, E., Garcia-Castillo, M.D., Arumugam, S., Chambon, V., Lamaze, C., Wunder, C., Kenworthy, A.K., et al. (2015). Endophilin-A2 functions in membrane scission in clathrin-independent endocytosis. Nature *517*, 493–496.

Sauvonnet, N., Dujeancourt, A., and Dautry-Varsat, A. (2005). Cortactin and dynamin are required for the clathrin-independent endocytosis of gammac cytokine receptor. J. Cell Biol. *168*, 155–163.

Subtil, A., Hémar, A., and Dautry-Varsat, A. (1994). Rapid endocytosis of interleukin 2 receptors when clathrin-coated pit endocytosis is inhibited. J. Cell Sci. *107*, 3461–3468.

Subtil, A., Delepierre, M., and Dautry-Varsat, A. (1997). An α-helical signal in the cytosolic domain of the interleukin 2 receptor beta chain mediates sorting towards degradation after endocytosis. J. Cell Biol. *136*, 583–595.

Suetsugu, S. (2016). Higher-order assemblies of BAR domain proteins for shaping membranes. Microscopy (Oxf.) *65*, 201–210.

Tang, Y., Hu, L.A., Miller, W.E., Ringstad, N., Hall, R.A., Pitcher, J.A., DeCamilli, P., and Lefkowitz, R.J. (1999). Identification of the endophilins (SH3p4/p8/p13) as novel binding partners for the beta1-adrenergic receptor. Proc. Natl. Acad. Sci. USA *96*, 12559–12564.

Taylor, M.J., Perrais, D., and Merrifield, C.J. (2011). A high precision survey of the molecular dynamics of Mammalian clathrin-mediated endocytosis. PLoS Biol. *9*, e1000604.